Protein-Containing PEGylated Cubosomic Particles: Freeze-Fracture Electron Microscopy and Synchrotron Radiation Circular Dichroism Study

ARTICLE *in* THE JOURNAL OF PHYSICAL CHEMISTRY B · JUNE 2012

Impact Factor: 3.3 · DOI: 10.1021/jp303863q · Source: PubMed

6 AUTHORS, INCLUDING:

Borislav Angelov
Academy of Sciences of the Czech Republic
51 PUBLICATIONS **945** CITATIONS
SEE PROFILE

Angelina Angelova
Université Paris-Sud 11
88 PUBLICATIONS **1,681** CITATIONS
SEE PROFILE

Brigitte Papahadjopoulos-Sternberg
NanoAnalytical Laboratory
43 PUBLICATIONS **1,443** CITATIONS
SEE PROFILE

THE JOURNAL OF PHYSICAL CHEMISTRY B

Article

pubs.acs.org/JPCB

Protein-Containing PEGylated Cubosomic Particles: Freeze-Fracture Electron Microscopy and Synchrotron Radiation Circular Dichroism Study

Borislav Angelov,[†] Angelina Angelova,*[,‡] Brigitte Papahadjopoulos-Sternberg,[§] Søren V. Hoffmann,[⊥] Valérie Nicolas,[#] and Sylviane Lesieur[‡]

[†]Institute of Macromolecular Chemistry, Academy of Sciences of the Czech Republic, Heyrovského nam. 1888/2, Praha 6, Czech Republic

[‡]CNRS UMR8612 Physico-chimie-Pharmacotechnie-Biopharmacie, Univ Paris Sud 11, LabEx LERMIT, 92296 Châtenay-Malabry, France

[§]NanoAnalytical Laboratory, San Francisco, California 94118, United States

[⊥]Institute for Storage Ring Facilities (ISA), Department of Physics and Astronomy, Aarhus University, Ny Munkegade 120, DK-8000 Aarhus C, Denmark

[#]Imaging platform, IFR141, Institut Paris-Sud d'Innovation Thérapeutique (IPSIT), Univ Paris Sud 11, 92290 Châtenay-Malabry, France

Supporting Information

ABSTRACT: The purpose of this work is to investigate the entrapment of protein molecules in cubosomic nanocarriers that are sterically stabilized by an amphiphilic poly(ethylene glycol) (PEG) derivative. Toward that aim, the mechanism of fragmentation of a self-assembled, PEGylated cubic lipid phase into nanoparticles (NPs) is investigated in excess aqueous medium. The molar ratio between the cubic-phase-forming lipid monoolein (MO) and its PEGylated derivative (MO-PEG_{2000}) is selected as to favor the formation of inverted-type liquid-crystalline (LC) structures (permitting one to reveal the stages of the fragmentation and bicontinuous membrane NP assembly process) rather than a phase transformation to lamellar or micellar phases. The PEGylated amphiphile considerably affects the interfacial curvature of the cubic lipid membrane and, under agitation, contributes to the fragmentation of the bicontinuous cubic lattice into NPs. Freeze-fracture electron microscopy (FF-EM), quasi-elastic light scattering (QELS), and confocal laser scanning fluorescence microscopy (CLSFM) are applied for determination of the NPs' sizes, inner organization, and stability with regard to a thermal stimulus. Entrapped protein molecules can essentially stabilize the cubosomic particles (proteocubosomes), which display well-defined inner organization of nanochannels in their freeze-fracture planes. The protein α-chymotrypsinogen A is studied in proteocubosome dispersions by means of far-UV synchrotron radiation circular dichroism (SRCD) spectroscopy. It is suggested that the protein molecules are entrapped in the interior of the PEGylated cubosomes via a "nanopockets" mechanism. The LC PEGylated proteocubosomes offer new possibilities for investigation of protein loading in sterically stabilized ("Stealth") nanostructured lipid carriers, which differ from Poloxamer-stabilized isasomes.

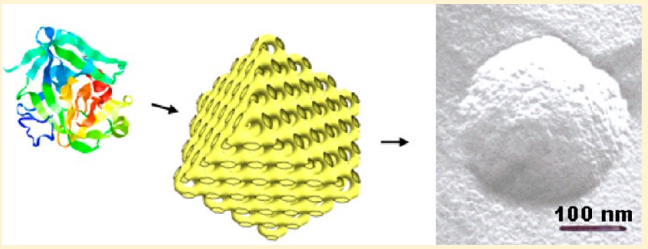

INTRODUCTION

High-resolution small-angle X-ray scattering (SAXS) investigations of the polymorphism and supramolecular structures of hydrated nonlamellar lipids and functionalized amphiphilic mixtures[1−14] have stimulated the interest in studies of new-generations lipid nanocarriers for loading, protection, and transport of drugs, peptides, therapeutic proteins (antibodies, enzymes), vitamins, cosmetic ingredients, and diagnostic agents.[15−30] Enhancement of the loading capacity and improvement of the controlled release and the bioavailability properties have been a permanent challenge in designing of nanostructured lipid-based carriers. As examples, multicompartment lipid vehicles have been obtained using molecular recognition reactions between complementary oligonucleotides anchored to liposomes[31] or by avidin−biotin bridges formed between neighboring vesicles.[32] Another approach toward increasing the drug encapsulation efficiency in lipid systems has involved the engineering of vesicular carriers, referred to as "vesosomes",[33] composed of numerous small vesicles encapsulated in a larger reservoir. Supramolecular engineering has also been employed for building up of multicompartment liposomes (MCLs), consisting of a small unilamellar vesicle (SUV)

Received: April 21, 2012
Revised: June 9, 2012
Published: June 21, 2012

Table 1. Terminology Used for Designation of Multicompartment Lipid Nanocarriers

term	NP organization	ref
vesosomes	Large vesicles encapsulating numerous small vesicles. (For a small number of encapsulated vesicles, vesosomes can be regarded as oligovesicular vesicles (OVVs).)	33
MCLs	Lipid particles involving two joint objects, for instance, a SUV separated from a MLV by an interface	34
DepoFoam particles	Multivesicular liposomes with a grape-like organization and micrometer dimensions	35
bilayer membrane-type particles	NPs built up of lipid bilayers. Depending on the packing symmetries/densities of the lipid bilayer membranes, these objects may be represented by cubosomes, spongosomes, onion-like liposomes, or vesicles.	16a
isasomes	Internally self-assembled somes. These particles can be of cubosome, hexosome, or spongosomes types depending on their inner organization. (Note that unilamellar vesicles are not isasomes, whereas hexosomes are isasomes but not bilayer membrane-type NPs.)	43a
nanocubosomes	Cubosomes in the range of 20−100 nm, which involve a few cubic unit cells. They do not display sharp Bragg diffraction peaks at variance to the bulk lipid phase.	21a

separated from a multilamellar vesicle (MLV) by an interface,[34] as well as of multivesicular liposomes called "DepoFoam" particles.[35] Table 1 includes a list of the terminology referring to multicompartment entities.

A different strategy for preparation of multicompartment lipid nanocarriers, displaying improved properties for drug entrapment and retention, has been the fragmentation of inverted-type liquid-crystalline (LC) bicontinuous cubic lipid phases by physical agitation and microfluidization in the presence of polymeric (e.g., Poloxamer) surfactants.[17,24,27] This approach can yield nanoparticles (NPs) with nonlamellar inner organizations,[26,27] which display essentially elevated interface areas as compared to traditional liposomes. The hydrophobic (membrane) and hydrophilic (aqueous channel) domains of the lipid NPs represent features typical for multicompartment vehicles.[16,17,24] Associated copolymer Pluronic (Poloxamer) surfactants or amphiphilic PEGylated stabilizers may provide steric barriers to the NPs' aggregation.[20,23,28]

Figure 1 schematically presents the nanochannel network organizations of inverted-type bicontinuous cubic and sponge membranous assemblies (a,b) and the corresponding NP types (c−f) that could be produced upon fragmentation of the bulk LC lipid phases in the presence of efficient hydrophilic stabilizers and high-energy input. It should be emphasized that for nonlamellar lipids, the resulting bilayer membrane-type particles (Figure 1c−f) include not only vesicles, formed by closed bilayers (Figure 1e), but also entities with diverse inner symmetries and lipid bilayer membrane packings that may belong to the "isasomes" class of nanocarriers (Table 1). The "bottom-up" study[22a] of the growth mechanism of cubic lipid NPs (Figure 1c) has found that only certain discrete states of the emerging bilayer membrane-type particles (with diameters divisible of a minimum size of around 54 nm) could be geometrically stable in configurations with open nanochannels. In fact, the bicontinuous double-diamond-type cubic lattice organization involves two networks of channels. The suggested mechanism of nanocubosome nucleation and growth predicts that the cubic lipid particles with closed channels could not be of stable configurations.[22a] In a "scaling-down" modeling, Covenay et al.[36] have indicated that the fragmentation of the bulk amphiphilic bicontinuous cubic lattice should be interrelated to the domain size, which is determined by the cubic unit cell size and the thermal fluctuations.

The steric stabilization of bilayer-membrane-type nanovehicles (Figure 1c−f) by PEGylation (using poly(ethyleneglycol) (PEG) surfactants), or by surface decoration with biocompatible amphiphilic copolymers, presents strong ongoing interest in relation to therapeutic and diagnostics applications.[15−17,19,20,23,24] PEGylation favors prolonged circulation of the lipid NPs in biological fluids. Factors that affect the bicontinuous LC NP formation, inner morphology, outer shape, and stability have been summarized by Barauskas et al.[27] The authors have used the dispersing agent Pluronic F127 in order to fragment bulk bicontinuous cubic and sponge LC phases of monoglyceride lipids and to kinetically stabilize them in the form of NPs. Structural X-ray diffraction (XRD) studies[23a,b] have established that the amphiphilic copolymer Pluronic F127 locates on the NP's surface. Therefore, the accessibility of the aqueous channels, located inside of the polymer-decorated cubosome NPs, for loading or releasing of guest (drug or protein) molecules needs to be further investigated.

Recently, the choice of dispersing agents for lipid cubic phases[16,19,20,28] has been extended to diverse amphiphilic macromolecular derivatives that are supposed to overcome the detected cytotoxicity of the Pluronic F127 detergent.[23c] For

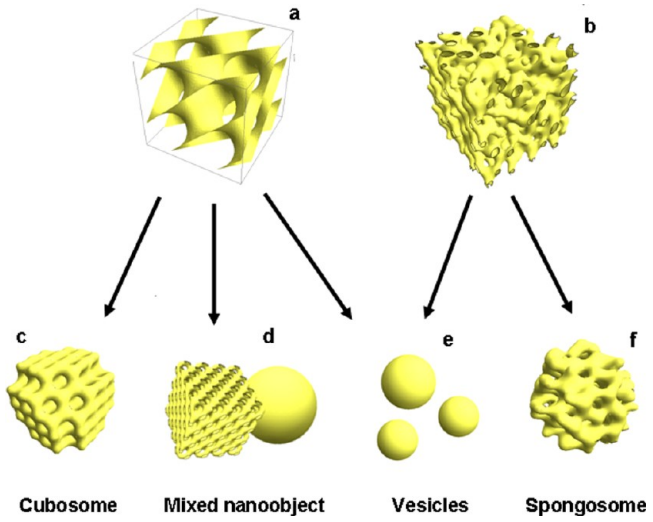

Figure 1. LC types of lipid nanocarriers resulting from the fragmentation of bulk inverted bicontinuous cubic ($Pn3m$) (a) or sponge (L_3) (b) mesophases; cubosome NP with a periodic cubic inner organization of lipid bilayers and a network of aqueous nanochannels (c); mixed (chimeric) nanoobject formed by joint cubic and vesicular (lacking inner channels) compartments (d); vesicular NPs consisting of closed lipid bilayers surrounding an aqueous core (e); spongosome NP droplet with a randomly curved, inner sponge-type bilayer membrane enclosing continuous water channels (f). These nanocarriers can be regarded as bilayer membrane-type particles as their internal organization involves packings of lipid bilayers. "Isasomes" would be a more generic term[43] for designation of the various internally self-assembled particles (somes) presented in the figure.

dx.doi.org/10.1021/jp303863q | J. Phys. Chem. B 2012, 116, 7676−7686

instance, biocompatible hydrophobic-anchored PEG polymer, starch, and hydrophobically modified cellulose (HMEHEC) have been included in the cubosome NPs formulations.[20a,b,24b] The cryo-TEM micrographs[20b] of the monoolein (MO)/HMEHEC dispersions have revealed a coexistence of various shaped multicompartment nanocarriers and mixed nanoobjects composed of joint vesicle and cubosome compartments (schematically presented in Figure 1d). While the monoglyceride lipid MO, characterized by a negative spontaneous monolayer curvature, has a preference for a cubic membrane packing (Figure 1a,c), the mixed surfactant-containing membranes appear to be less curved and show a tendency toward bilayer vesicle formations (Figure 1e). Hence, the inhomogeneous distribution of the membrane curvature throughout the generated dispersed lipid NPs results in the formation of mixed objects such as cubosomes and vesicles fused into one aggregate[20] (Figure 1d). Experiments aiming at preparation of cubic LC NPs via fragmentation of bulk bicontinuous inverted cubic phases of monoglyceride lipids have shown that the Poloxamer-stabilized cubosome NP's population, obtained at ambient temperature, is often accompanied by vesicles.[17,24a] The vesicular NP's population (Figure 1e) has been especially pronounced when the agitation of the lipid/Poloxamer system has been done by powerful ultrasonication and by homogenization using a high-pressure microfluidizer. Thus, the monoglyceride NP dispersions may contain a variety of transient multicompartment structures and mixed chimeric (i.e., consisting of two different moieties) nanoobjects, which coexist with cubosomes and several vesicles.

On the other side, the dispersion of the bicontinuous sponge phase containing the glycolipid mannosyl-erythritol lipid-A and the phospholipid L-α-dilauroylphosphatidylcholine (DLPC) has resulted in the production of a thermodynamically stable population of vesicles.[30a−c] The NP interfaces have been stabilized by hydrogen-bonding-network interactions between the sugar head groups of the employed nonionic amphiphile.[30a] Depending on the DLPC molar fraction, a coexistence of vesicles and sponge (L_3 phase) objects (Figure 1f) could be found in the aqueous dispersions.[30b,c] This event represents an analogy with the established coexistence of cubic phase NPs and vesicles in excess water.[24a,b] At very low percentages of DLPC in the lipid mixture, droplets with characteristic sponge (L_3) phase morphology (i.e., random 3D networks of lipid bilayers) have formed.[30c,d]

In the present work, we investigate the mechanism of NP formation from a PEGylated bicontinuous inverted cubic phase of the nonionic lipid MO that entraps soluble protein (α-chymotrypsinogen A) molecules. A PEGylated amphiphile, MO-PEG_{2000}, is included in the hydrated nonlamellar nanostructure in order to induce modifications in the lipid bilayer curvature and packing and to facilitate the fragmentation (upon vortexing) of the bicontinuous cubic membrane into kinetically stabilized NPs. The molecular weight of the PEG moiety is fixed to PEG2000, taking into account the capacity of the PEG2000 chains to hinder the lipid NPs aggregation under physiological conditions.[37] The formation mechanism of PEG-functionalized MO NPs, in the absence and in the presence of protein molecules, is studied by means of freeze-fracture electron microscopy (FF-EM)[21] and quasi-elastic light scattering (QELS).[15b] Synchrotron radiation circular dichroism (SRCD)[38−41] spectra are acquired for the investigated protein α-chymotrypsinogen A in solution and in lipid NP dispersions. The recent UV−VUV SRCD method[41] appears to be appropriate for this kind of experiments as the traditional CD spectrometers could not measure the relevant CD signals of the protein in the far-UV spectral region due to significant scattering of the lipid nanocarriers (masking the protein bands at wavelengths below 300 nm). The responsiveness of the LC NPs to external stimuli is evidenced by CLSFM[42] imaging. The challenges in preparation of protein-containing sterically stabilized LC lipid NPs are discussed.

MATERIALS AND METHODS

Materials and Samples Preparation. MO powder (1-monooleoyl-rac-glycerol, C18:1c9, MW 356.54, purity 99.5%), the fluorescence probe Nile Red (Fluka Standard, MW 318.38), the protein α-chymotrypsinogen A (25.7 kDa, salt-free, lyophilized powder, type II from bovine pancreas, purified by 6× crystallization), and the solvents chloroform, ethanol, and methanol were purchased from Sigma-Aldrich (Saint-Quentin, France). The poly(ethylene glycol)monooleate NHS derivative (MO-PEG_{2000}, MW 2104, BAM Sunbright OE-020CS) was purchased from the NOF Corporation (Tokyo, Japan). The nonionic amphiphile MO-PEG_{2000} is weakly soluble in aqueous medium. At concentrations above its critical aggregation concentration (CAC), which is around 1×10^{-5} M in a phosphate buffer, it forms PEGylated micellar-type aggregates with a mean hydrodynamic diameter of 8 nm as determined by QELS. Phosphate buffer solution (1×10^{-2} M, pH 7) was prepared using the inorganic salts NaH_2PO_4 and Na_2HPO_4 (p.a. grade, Fluka, Saint-Quentin) and Milli-Q water (Millipore Co., Molsheim).

LC lipid NPs preparations were obtained by the method of hydration of a dry lipid film followed by physical agitation. The mixed amphiphilic films were composed of MO and MO-PEG_{2000} in desired proportions. The organic solvent (chloroform/ethanol, 3/1 v/v) was evaporated under a flow of nitrogen gas, and the resulting binary mixtures were lyophilized overnight. For confocal laser scanning fluorescence microscopy (CLSFM) studies, the samples were labeled by the fluorescent probe Nile Red at a dye/lipid molar ratio of 1/100. The lipophilic dye was added as a chloroform solution to the lipid mixture before the solvent evaporation that yielded a lipid film. The lipid assemblies were initially incubated with an excess aqueous buffer phase for 30 min followed by repeated vortexing. Subsequently, 5−10 min of sonication was performed in ice medium using a sonication bath with a moderate frequency (40 kHz, Branson 2510) (Branson Ultrasonics, Geneve). The MO-PEG_{2000} amphiphile served as a solubilizing and a dispersing agent of the MO cubic phase. It facilitated the fragmentation of the bulk LC (MO/MO-PEG_{2000}/buffer) structures into kinetically stabilized NPs. Any nondispersed fractions of the binary self-assembled amphiphilic mixtures were removed by filtering through a 0.22 μm Millipore filter (Minisart HighFlow, Sartorius, Palaiseau). The lipid concentration in the prepared stock NP dispersions was ~20 mM.

The ability of the PEGylated MO-based nanoparticulate carriers to upload protein macromolecules in their inner structure was studied using the protein α-chymotrypsinogen A. Protein-containing NPs were prepared by dissolving α-chymotrypsinogen A (MW 25.7 kDa) in the aqueous buffer phase used for hydration of the lyophilized mixed lipid (MO/MO-PEG_{2000}) film. The protein stock solution concentration was 4 mg/mL in a phosphate buffer. The physical agitation of the self-assembled MO/MO-PEG_{2000}/protein mixture con-

dx.doi.org/10.1021/jp303863q | J. Phys. Chem. B 2012, 116, 7676−7686

sisted of 10 vigorous vortexing cycles. Ultrasonication was not recommended as it may perturb the native protein folding. It should be emphasized that the presently reported preparation of protein-loaded LC lipid nanocarriers differs from the methodologies in which the biomacromolecule is incubated with a solution of preformed lipid vehicles.[16b]

Quasi-Elastic Light Scattering (QELS). The particles size distributions in the investigated LC lipid dispersions were determined using a nanosizer apparatus (Nano-ZS90, MALVERN, Orsay) equipped with a helium−neon laser of 633 nm wavelength. The samples were diluted to a 1 mM lipid concentration prior to measurement in 1 cm thick cells and analyzed in an automatic mode using the following experimental parameters: temperature 25 °C; scattering angle, 90°; refracting index, 1.33; environment medium viscosity, 0.890 cP. The average hydrodynamic diameter, d_h, was calculated considering the mean translational diffusion coefficient, D, of the particles in accordance with the Stokes−Einstein law for spherical particles in the absence of interactions, $d_h = k_B T/3\eta\pi D$, where k_B is the Boltzmann constant, T is temperature, and η is the viscosity of the aqueous medium. Three measurements with the same cell were averaged for every sample. The results were analyzed using the MALVERN Zetasizer software (version 6.11) and presented as volume statistic distribution plots of the particles hydrodynamic diameters. The plotted maximal intensities (volume %) correspond to the mean NP sizes, which are most abundant in the sample.

Confocal Laser Scanning Fluorescence Microscopy (CLSFM). For CLSFM imaging, the sample concentration was 1/10 of that of the stock NP preparation. The solution (20 μL) of NPs, labeled by Nile Red, was examined under a microscope using a supporting cell of two glass slides (MENZEL-GLÄSER, Braunschweig, Germany). The fluorescence micrographs were recorded in a scanning mode at the platform "Cellular Imaging" (IFR 141-IPSIT). The setup consisted of a confocal microscope Zeiss LSM-510 (Carl Zeiss, Le Pecq) operated with a Plan Apochromat oil immersion objective lens (magnification 63×, numerical aperture NA 1.40) and using a 1 mW helium−neon laser. The excitation wavelength for the Nile Red dye was λ_{ex} = 543 nm. A long-pass emission filter LP560 was employed to take the confocal fluorescence micrographs under 543 nm laser illumination and at a pinhole diameter of 106 μm. Fluorescence was collected at emission wavelengths of λ_{em} > 560 nm. The imaged particles were visualized by the LSM image browser software (Carl Zeiss, Oberkochen).

Freeze-Fracture Electron Microscopy (FF-EM). Electron micrographs were taken from several freeze-fracture preparations of relatively concentrated NP dispersions (~20 mM lipid) as well as from 1/10 diluted dispersions. For FF-EM, the samples were quenched using a sandwich technique and liquid-nitrogen-cooled propane. Using this technique, a cooling rate of 10 000 K per second was reached, avoiding ice crystal formation and artifacts possibly caused by the cryofixation process. The cryofixed samples were stored in liquid nitrogen for less than 2 h before processing. The fracturing process was carried out in JEOL JED-9000 freeze-etching equipment, and the exposed fracture planes were shadowed with Pt for 30 s at an angle of 25−35° and with carbon for 35 s (2 kV/60−70 mA, 1×10^{-5} Torr). The replicas produced this way were cleaned with concentrated, fuming HNO_3 for 24 h followed by repeated agitation with fresh chloroform/methanol (1:1 by volume) at least five times. The cleaned replicas were examined at a JEOL 100 CX electron microscope (NanoAnalytical Laboratory, San Francisco).

Synchrotron Radiation Circular Dichroism (SRCD) Spectroscopy. SRCD spectra of the protein α-chymotrypsinogen A were studied in the far-UV wavelength region from 170 to 260 nm at the UV−VUV CD1 beamline of the synchrotron radiation source ASTRID[38] at the Institute for Storage Ring Facilities (ISA) (Aarhus University, Denmark). Sample and baseline spectra were collected in a circular quartz cell (Hellma, GmbH) with a cell path length of 0.1 mm (the required sample volume was ~25 μL). A temperature-controlled sample holder was employed. The geometry of the latter assured that the circular cell was always positioned in the same orientation with respect to the incoming beam. The beam spot was of a rectangular shape, and the beam size on the sample was ~6×2 mm^2. The distance between the sample and the PMT detector was less than 3 cm. The cell chamber was continually purged with dry nitrogen gas (5 L/min). The setup was calibrated for wavelength and optical rotation magnitude using a camphorsulfonic acid (CSA) standard solution (~10 mg/mL) and a two point calibration in the spectra recorded from 170 to 350 nm. The baselines and the spectra of the samples were acquired using six consecutive scans, in 1 nm increments, and a 2.15 s dwell time per wavelength. Baselines were recorded with sodium phosphate buffer, which was degassed under vacuum to remove the air bubbles. The same phosphate buffer aqueous solution was used for sample preparation. Salts, like NaCl, were avoided in these spectroscopic experiments as their absorption, at wavelengths below 210 nm, perturbs the recording of the protein bands in the far-UV region.[38,39] The protein CD spectra were measured at 25 °C in the presence and absence of LC lipid NPs. Dilutions were done to a final protein concentration of 1 mg/mL. The baseline of the "blank" lipid NP dispersions (without entrapped proteins) was subtracted from the far-UV CD spectra of the NP samples containing α-chymotrypsinogen A. The SRCD data were processed using the CDtool software.[39d] The measurements of six consecutive scans were averaged, corrected for baseline signals, slightly smoothed with a Savitzky-Golay filter, and calibrated by CSA. The spectral intensities were expressed in per residue molar absorption units of circular dichroism (delta epsilon units) and analyzed toward determination of the protein secondary structure content. The SVD (single-value decomposition) calculations[39d] were iterated until a convergent solution was achieved.

RESULTS AND DISCUSSION

Formation of PEGylated Self-Assembled Nanovehicles of Hydrated MO. Depending on their molar fraction in the lipid mixtures, PEGylated MO derivatives may essentially influence the overall temperature-dependent structural phase behavior[10a] of the hydrated monoglyceride lipid. In preliminary experiments on functionalization of the MO cubic phase by the PEGylated amphiphile MO-PEG$_{2000}$, the molar ratio between the lipid and surfactant components was varied in the sequence 99/1, 98/2, 97/3, and 95/5 (mol/mol) in order to search for conditions permitting LC cubic NP formation in an excess phosphate buffer phase. The time-resolved synchrotron radiation small-angle XRD study (see Figure 1S in the Supporting Information) established that the bulk cubic lattice organization of the monoglyceride lipid (MO) was preserved at low molar fractions of the PEGylated derivative (MO-PEG$_{2000}$). However, the initial diamond-type ($Pn3m$ space group) cubic

dx.doi.org/10.1021/jp303863q | J. Phys. Chem. B 2012, 116, 7676−7686

structure of the hydrated MO was modified depending on the percentage of the PEGylated surfactant. The coexistence with *Im*3*m* cubic domains revealed that the membrane hydration and curvature strongly depend on the lipid composition and temperature[7a,43] and suggested the possibility for generation of mixed type and core−shell nanostructures. With the increase of its molar fraction in the system, the PEGylated amphiphile MO-PEG_{2000} decreases the average packing parameter of the self-assembled lipid mixture, and a transition to intermediate or lamellar phases could occur.[10a]

In this work, LC samples with mixed lipid compositions MO/MO-PEG_{2000} 99/1 and 98/2 (mol/mol) were selected for the FF-EM investigation of the NPs' formation (Figures 2 and 3). The FF-EM micrographs, taken from the as-prepared nondiluted sample MO/MO-PEG_{2000} 99/1 (mol/mol), show the presence of numerous small NPs with sizes in the range from 20 to 120 nm (see also Figure 2S in the Supporting Information). The dominating portion of the PEGylated NPs has a mean diameter of around 60 nm (Figure 2a).

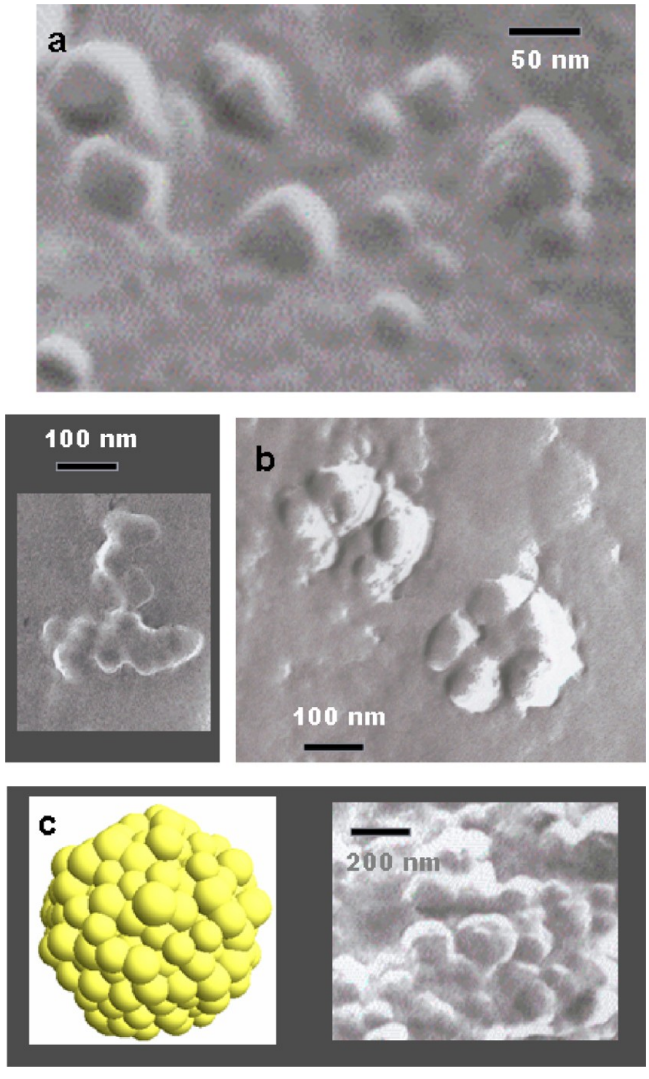

Figure 2. FF-EM images taken from a relatively concentrated dispersion (~20 mM lipid) of NPs formed by a self-assembled MO/MO-PEG_{2000} 99/1 (mol/mol) mixture in 10^{-2} M phosphate buffer. (a) Magnified fracture plane showing small, individual NPs; (b) aggregates of a grape-shape formed upon storage by bridging of LC NPs bigger than 200 nm in diameter (the storage time was about two weeks); (c) modeling of a grape-shape cubosomic cluster, in which the joint NPs are relatively large (>200 nm) and they are not wholly fused.

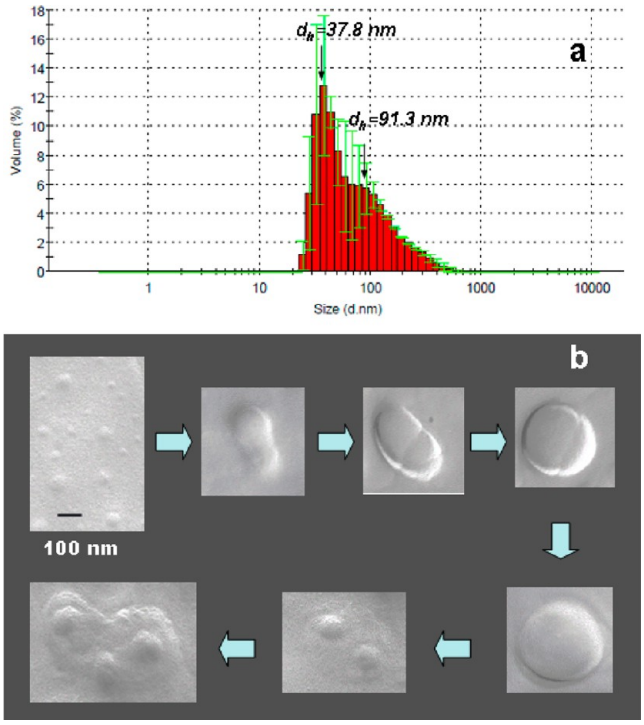

Figure 3. (a) QELS determination of the mean hydrodynamic diameters of LC NPs in a MO/MO-PEG_{2000} 98/2 (mol/mol) system dispersed by vortexing and sonication and diluted 10 times in a phosphate buffer. The measurement is performed at 25 °C. The volume distribution plot of the NP's sizes shows two populations of NPs. The error bars are indicated in green. (b) FF-EM images showing the possible growth stages of the LC NPs in a dispersed MO/MO-PEG_{2000} 98/2 (mol/mol) sample after 10 times dilution and equilibration in 10^{-2} M phosphate buffer. Images are taken from parallel events in the sample. The bar corresponds to 100 nm. The aggregate size reaches ~400 nm.

The performed FF-EM analysis showed that all NPs investigated in this study display their shadows behind their structures mostly. Typically, liposome particles display concave (shadow in front) and convex (shadow behind their structures) fracture planes.[44] Concave fracture behavior, representative of vesicles enclosing large aqueous cores, is not characteristic of the investigated sample (Figure 2a). Taking into account the small sizes of the obtained PEGylated nanoobjects, a question arose whether the prepared NPs could be identified as small vesicles or as nanocubosomes that may progressively aggregate into grape-shaped clusters in concentrated systems (Figure 2b,c). The FF-EM imaging established that the small particles appear to contribute to the formation of larger particles (see the parallel fusion events presented in Figure 3b). At ambient temperature, only a few larger NPs, with diameters, *d*, between 380 and 520 nm, were observed as individual aggregates (Figure 2b). A minor fraction of self-assembled aggregates with a hydrodynamic diameter of around 400 nm was detected by QELS.

The results of the QELS investigation (Figure 3a) demonstrate that the volume distribution of NP populations is in agreement with the FF-EM results. The major volume fraction of LC NPs displays small average sizes ($d_h \approx 40$ nm). Larger nanovehicles with hydrodynamic diameters, d_h, between 90 and 400 nm are present as coexisting objects resulting from

dx.doi.org/10.1021/jp303863q | *J. Phys. Chem. B* 2012, 116, 7676−7686

the cubic phase fragmentation. Equilibrium between the two NPs' populations can be deduced.

Figure 3b presents magnified FF-EM images of NPs in a 10× diluted sample of MO/MO-PEG$_{2000}$ 98/2 (mol/mol). The first image shows that the colloidal dispersion is characterized by a high content of small NPs ($d \leq 80$ nm). Some of these small NPs tend to merge into bigger ones. As a consequence, one observes also chimeric-type nanoobjects (joint particles) (Figure 3b). The NP fusion events were recorded in parallel, which confirms that the small NPs contribute to the formation of larger particles ($d \leq 560$ nm). The two coexisting populations of NPs are a typical feature for this molar composition as well (Figure 3). The freeze-fracture shadows, which are present behind the growing objects, are characteristic of the MO-based LC particles. Moreover, the increased quantity of the PEGylated agent, MO-PEG$_{2000}$, favors the formation of a PEG corona sterically stabilizing the NP's surface. The comparison of the NPs' morphologies in Figures 2a and 3b indicates that the augmented fraction of the PEGylated component confers a smoother and soft nature of the NPs' interfaces. The particles look liquid-like as they are covered by a soft polymer shell.

With the investigated PEGylated mixture here, the MO NP formation mechanism seems to be different from the "core–shell" model proposed by Nakano et al[23a] (in particular, for cubosomes stabilized by a Pluronic copolymer). In the present case, the MO-PEG$_{2000}$ amphiphile appears to laterally mix in the lipid membrane and hence may not be only surface-exposed as a shield on the NP surface.

The FF-EM study revealed that the numerous small NPs (initial size ≈ 55 nm) can grow via intake of membrane fragments that are present in the dispersed liquid phase after the sonication of the cubic MO/MO-PEG$_{2000}$/buffer mixture. When the growing LC NPs become large enough (ca. 200–300 nm), they begin to form clusters of a grape shape (Figure 2c). On the other hand, Figure 2a clearly shows that the very small NPs stay apart and do not aggregate into grape-shaped clusters. Therefore, the PEGylated NPs are sterically stable and should first reach sufficiently big sizes before being able to aggregate into clusters. The image in Figure 2b confirms that a complete fusion between the NPs does not occur as they are partially surface-decorated by PEG chains, which serve as steric stabilizers against aggregation. Considering that the PEGylated component, MO-PEG$_{2000}$, constitutes less than 2 mol % in the amphiphilic assemblies (i.e., it is of insufficient quantity to spread over the entire NP surface), it could be suggested that clustering of lipid NPs would be possible when they adhere by bridging of non-PEGylated areas exposed on their surfaces.

Stability of the PEGylated Nanovehicles of MO with Regard to Thermal Stimuli. NPs of LC fluid nature (MO/MO-PEG$_{2000}$, 98/2 mol/mol) were imaged by CLSFM. The CLSCM study permitted demonstration of the thermal sensitivity and the response of the NPs to local heating due to laser illumination. In these experiments, the confocal imaging employed a focused laser beam, which produced spotted heating on the dispersed NPs sample. The effect of the thermal shock on the NP's organization during laser scanning is presented in Figure 4. The first imaging scan revealed the presence of small NPs (Figure 4a) with uniform sizes. A change of the NP's population was established upon continuous laser scanning.

During the consecutive laser scans, growing spherical droplets were observed (Figure 4b,c). Such effects have not been reported for lamellar phase liposomes (e.g., formed with egg PC/DSPE-PEG$_{2000}$ phospholipids mixtures).[37] Normally, vesicles do not swell up to micrometer sizes upon heating, but they can transform into nonlamellar structures with inner organization (such as cubosomes).[11c] The increase in the

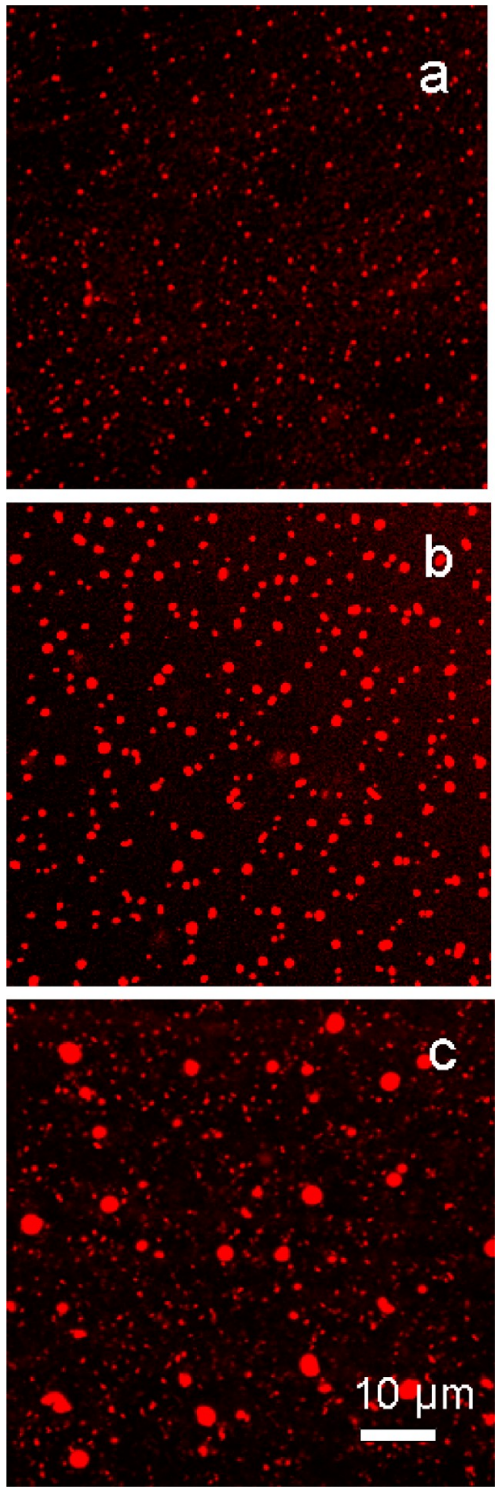

Figure 4. Confocal laser scanning fluorescence micrographs (CLSFMs) of dispersed PEGylated monoglyceride particles (MO/MO-PEG$_{2000}$, 98/2 mol/mol) labeled by Nile Red. The fluorescent dye is preferentially incorporated in the lipid membrane. (a) Image taken upon the first laser scan over the NPs sample; (b) image after the second laser scan; (c) image obtained after 2 min of laser scanning.

dx.doi.org/10.1021/jp303863q | J. Phys. Chem. B 2012, 116, 7676–7686

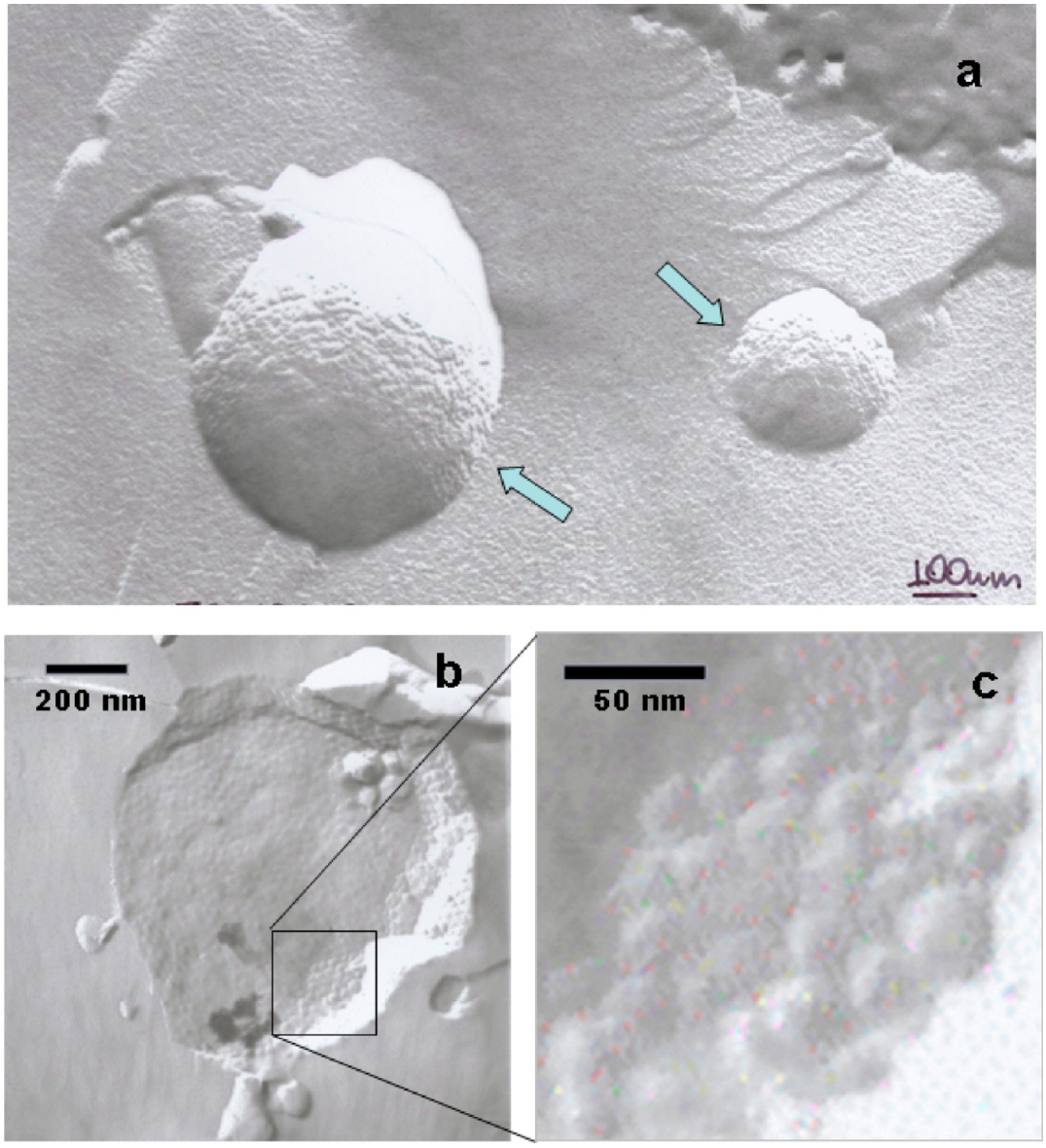

Figure 5. FF-EM images showing the surfaces (a) and the cross sections (b,c) of PEGylated proteocubosome particles with an inner cubic organization of nanochannels. The MO/MO-PEG_{2000} (98/2 mol/mol) lipid mixture was incubated with the protein α-chymotrypsinogen A (4 mg/mL solution in 10^{-2} M phosphate buffer) before vortexing that yielded LC particles upon dispersion. The arrows indicate two PEGylated proteocubosome particles (convex fractures).

particle size due to the thermal shock taking place on the NPs can be interpreted by the natural tendency of the cubosomes to form larger structures via minimizing the exposed surface area. The small cubosome particles represent kinetically stabilized dispersions with a large surface-area-to-volume ratio. However, the bulk cubic LC phase is a thermodynamically more stable assembly as compared to its dispersed fragments. It should be recalled that large LC domains, with their greater volume-to-surface-area ratio, represent a lower-energy state.[45] This promotes the recovery of large LC cubic particles upon heating. The observed increase in the size of the dispersed particles due to laser illumination might be similar to that observed upon heating oil-in-water emulsions stabilized by nonionic stabilizers[46] and also to the effect of light illumination on inducing lamellar−nonlamellar transition in lipid/gold NP aqueous dispersions.[47] In fact, heating to elevated temperatures of nonionic oil-in-water emulsions enhances their destabilization due to coalescence. Figure 4 indicates that the local heating shock, applied to the aqueous dispersion, induces coalescence of the small particles, producing bigger particles. In addition, it should be taken into account that the hydrophilic head groups of the lipids are dehydrated during heating.[46] It seems that the PEGylated lipid loses its efficiency as a stabilizer with increasing temperature due to the dehydration of the PEG chains.

The performed SAXS measurements confirm that the bulk nonlamellar lipid phase is favored for this amphiphilic mixture. The nonlamellar Bragg peaks are well-defined in the SAXS patterns at elevated temperatures (see Figure 1S in the Supporting Information). These structural features should be taken into account when aiming at protein encapsulation in such LC nanostructures.

Formation and Stability of PEGylated Proteocubosomes. The "proteocubosomes" class of nanostructures represents protein-entrapping soft materials with multicompart-

dx.doi.org/10.1021/jp303863q | J. Phys. Chem. B 2012, 116, 7676−7686

ment LC organization.[9c,16a,21,22] They can be generated from bulk cubic lipid phases, which are incubated with protein molecules and subjected to subsequent fragmentation. The proteins, encapsulated in a cubic lipid network assembly, may have profound structural influence on the host amphiphilic phase and on the formation of hierarchically organized domains, patterns, or intermediates.[7c,11a,21] Depending on their size and hydrophobic/hydrophilic balance, proteins can facilitate the fragmentation and dispersion of the bulk LC lipid phase.[16a,21a]

Toward the aim of preparing PEGylated proteocubosomes, we investigated a self-assembled mixture of the amphiphiles MO and MO-PEG$_{2000}$ and the protein α-chymotrypsinogen A. The protein was incubated with the lyophilized lipid film at an initial concentration of 4 mg/mL. The self-assembly method was employed in order to favor the protein entrapment in the 3D network structure rather than its repulsion from the stealth NP surface. The QELS measurements established that the mean hydrodynamic diameter of the solvated α-chymotrypsinogen A is d_h = 4.8 nm (see Figure 6b) and that this protein does not cluster into large aggregates under the investigated temperature and phosphate buffer conditions. It was taken into account that the hydrodynamic diameter of α-chymotrypsinogen A is comparable with the aqueous nanochannel sizes[7c] in MO-based cubosomic vehicles (3−7 nm). Therefore, the uploaded protein can be expected to be entrapped in a nanoconfined state in the lipid NP assemblies. The proposed "nanopockets" mechanism[7c,21a] of protein encapsulation can be suggested to be pertinent to this system as well.

Figure 5 shows FF-EM images of a MO/MO-PEG$_{2000}$ (98/2 mol/mol) sample self-assembled in the presence of α-chymotrypsinogen A molecules. In contrast to the NP samples without protein (Figures 2 and 3), this preparation (obtained with little energy input) displays a few small NPs (d∼30 nm) and many large particles of submicrometer sizes (see also Figure 6a). A number of these protein-loaded particles show a distinct inner fine structure. Cross fractions, obtained with relatively large nanovehicles of submicrometer sizes, are hierarchically organized and consist of assemblies of nanocubosomes (Figure 5, bottom panels). These cross sections expose a regular internal structure involving networks of nanochannels. The inner cubosome architecture is well-defined in the freeze-fracture plane presented in Figure 5 (panels b and c). The entrapped protein seems to be able to form bridges between the nanocubosome subunits and to favor the LC particle formation involving inner network structures.

A particularity of the system investigated here is that the sterically stabilized cubosome NPs possess a soft corona of PEG polymer chains (Figure 5a). The surfaces of the proteocubosome particles appear to be rather smooth. The study revealed that the internal organization of the NPs is cubosomal, as shown in the FF-EM image (Figure 5b), whereas the outer NP surface corresponds to a soft interface (Figure 5a). It can be recalled that the functionalization of the diamond-type cubic lipid particles by macromolecules could lead to interfacial structuring of the cubosomal objects and may lead to prolate or oblate droplet shapes.[21a] While the entrapped nanoconfined protein appears to stabilize the inner NPs' structure of a cubic type, the amphiphilic PEGylated agent (MO-PEG$_{2000}$) creates a fluid-like layer on the proteocubosome surface, adopting soft, droplet-like shapes.

The QELS investigation of the proteocubosome sample (Figure 6a) determined the average hydrodynamic diameters of

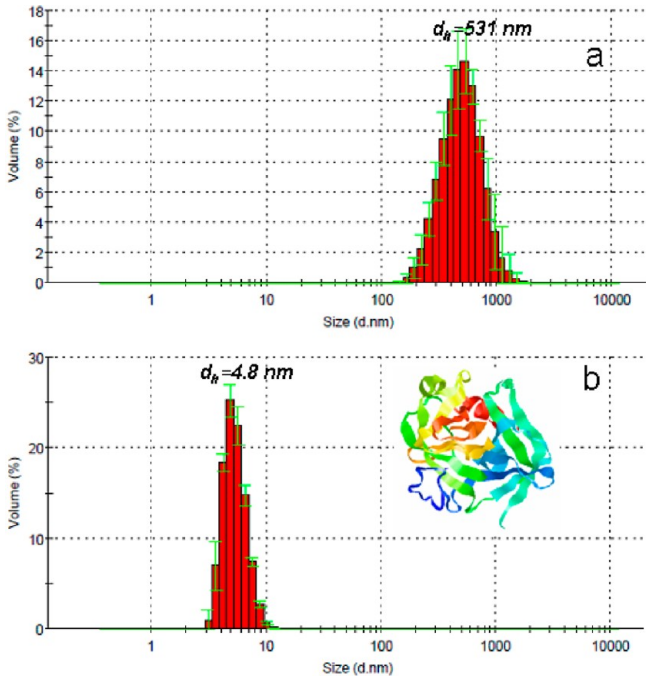

Figure 6. QELS determination of the particle sizes in (a) a proteocubosome MO/MO-PEG$_{2000}$ (98/2)/α-chymotrypsinogen A system dispersed in excess 10^{-2} M phosphate buffer phase and in (b) stock solution of bovine pancreatic α-chymotrypsinogen A (c = 4 mg/mL). (Inset) The α-chymotrypsinogen A structure (PDB code: 1CHG). The QELS measurements are performed at 25 °C. The error bars are indicated in green.

the dispersed NPs. The obtained mean d_h values, in the range between 220 and 720 nm, are in agreement with the FF-EM results (Figure 5). One can note the larger hydrodynamic dimensions of the α-chymotrypsinogen-A-entrapping LC particles as compared to the "empty" LC nanocarriers. In fact, the protein-lacking NPs (Figure 3) were produced with more powerful physical agitation (sonication in an ice bath) applied to fragment the bulk MO/MO-PEG$_{2000}$ (98/2, mol/mol) LC mixture. Evidently, the vigorous physical agitation favors the formation of smaller-size NPs.

Figure 6a demonstrates that the large NPs (mean $d \approx$ 530 nm) are dominating the size distribution of the nanovehicles entrapping protein molecules. Because the volume portion of large particles, displaying inner fine structures, is larger than that of the smaller NPs, it can be supposed that the encapsulated protein macromolecules help bridge the non-PEGylated exposed membrane areas into a supramolecular, nanocubosomal structure with aqueous channel networks (Figure 5c). The QELS study demonstrated that free protein molecules, with d_h = 4.8 nm (Figure 6b), are not detectable in the volume distribution graph of the proteocubosome sample (Figure 6a). This suggests that the amphiphilic α-chymotrypsinogen A is preferentially entrapped in the interior of the nanostructured lipid particles.

The effect of the PEGylated lipid nanocarriers on the secondary structure conformation of α-chymotrypsinogen A, entrapped in proteocubosomes preparations, was investigated by far-UV SRCD spectroscopy. The SRCD is the main method to assess CD bands at low wavelengths, providing new insights into the interaction of proteins with lipid assemblies. In principle, the CD bands in the far-UV spectral region from 180 to 260 nm may be assigned to protein secondary structure

dx.doi.org/10.1021/jp303863q | J. Phys. Chem. B 2012, 116, 7676−7686

categories involving α-helices, β-sheets, turns, and unfolded conformations. The SRCD technique, investigating lipid-phase-associated proteins, may derive secondary structure information that could involve mixtures of conformational states. It may distinguish whether the protein is disordered in a solution phase, in the lack of lipid NPs, and whether it may fold into more (or possibly less) ordered structures upon entrapment within the lipid nanovehicles. This kind of investigation could not be performed with a conventional CD instrument, owing to the strong scattering and absorption of the LC lipid nanoobjects displaying relatively dense internal membrane structure. In contrary, SRCD has been shown to be well-suited for studies of proteins in scattering samples.[41]

Figure 7 compares the far-UV SRCD spectra of α-chymotrypsinogen A, entrapped in a nanoparticulate dispersion

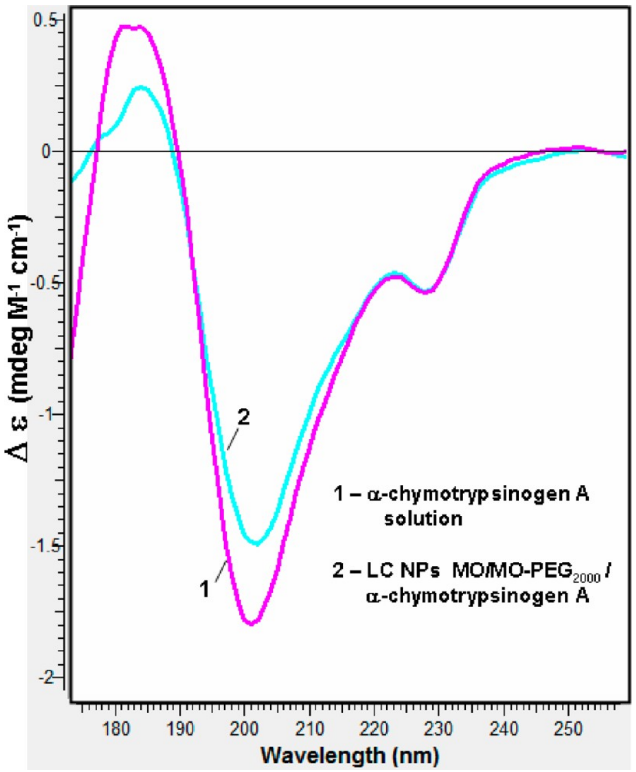

Figure 7. Far-UV SRCD spectra of the protein α-chymotrypsinogen A measured in solution (c = 1 mg/mL) (1) and in aqueous dispersion of LC NPs (MO/MO-PEG$_{2000}$, 98/2 mol/mol) loaded with the protein (2). Aqueous phase: 10^{-2} M phosphate buffer. The spectra were acquired after sample equilibration at a temperature of 25 °C.

of LC MO/MO-PEG$_{2000}$ vehicles, and of the free protein in solution. The observed main features in the spectra are the negative peak at 201 nm, a shoulder at 229 nm, and a weak positive signal at 185 nm. It is apparent that the obtained far-UV CD spectra differ from those of α-helical proteins, which display rather strong positive intensities at a wavelength of ~190 nm and two negative bands at ~208 and ~222 nm. A more close resemblance is found with the shape of the CD spectra of unstructured proteins (displaying a negative peak at wavelengths below 210 nm) and with those of proteins with β-sheet and β-turn secondary structure contents. The β-sheet protein structure formation can be evidenced by a negative minimum at 215 nm and a relatively weak positive band at 198 nm. Regarding the intensity of the SRCD spectra presented in Figure 7, it can be noted that the nanoconfined α-chymotrypsinogen A molecules, uploaded in the LC lipid NP dispersion, display a smaller CD signal as compared to that of the free protein in buffer solution. This indicates that the NP preparation procedure, the resulting protein nanoconfinement, or interactions with the constituents of the PEGylated lipid nanovehicles influences the secondary structure content of the encapsulated protein.

The performed SVD analysis of the SRCD spectra, implemented in the CDTool software[39d] (using the SELCON2 algorithm), permitted determination of the secondary structure content of α-chymotrypsinogen A in the investigated buffer phase as well as in the NP solution. Under the employed experimental conditions, the total percentage of β-sheets and β-turns in the α-chymotrypsinogen A solution structure (spectrum 1 in Figure 7) was determined to be around 50%, whereas 9% was fitted by α-helices and 41% were assigned to "other" conformations. For the α-chymotrypsinogen A entrapped in a dispersion of LC lipid NPs (spectrum 2 in Figure 7), the refinement procedure yielded a reduced β-sheet and β-turn percentage (37–40%). Thus, the conformation of both the soluble and encapsulated protein is dominated by coexisting β-sheet and β-turn structures with a large percentage of statistical conformations of "other" type. It can be deduced that the protein nanoconfinement in the 3D nanochannel network structure, or the association of the protein molecules to the lipid bilayers, slightly alters the protein folding. However, evidence for protein aggregation was not obtained in this work.

CONCLUSION

The performed study revealed that the fragmentation of the PEGylated bulk lipid cubic assembly typically yields two populations of NPs at ambient temperature. One of them is considered to represent MO bilayer membranes and fragments, which merge into multicompartment structures. The second one consists of larger LC nanocarriers with inner channel organization (as a precursor of the bulk lipid cubic phase). The coexistence of small vesicles with growing cubosome particles in the kinetically stabilized MO/MO-PEG$_{2000}$ LC NP system should be considered as a general feature at room temperature. Independently of the chemical nature of the amphiphilic stabilizer, the cubosome–vesicle coexistence has been documented also in Poloxamer-stabilized lipid dispersions.[24a]

The CLSFM imaging established that the cubosome particle coalescence and growth is facilitated by a thermal stimulus, the bulk nonlamellar LC phase of the lipid mixture being a thermodynamically more stable state at elevated temperatures. Therefore, it can be concluded that the small NPs serve as building units for the larger cubosomal particles observed upon heating. The steric stabilization of the NPs by a PEG corona is associated with smoothing of the cubosomic interfaces. The PEG-functionalized NPs appear as liquid-like droplets in the obtained FF-EM images, rather than as rigid crystalline nanoporous cubic lattice objects. The far-UV SRCD results indicate that the protein uploading and nanoconfinement in fragmented, nanoparticulate cubic assemblies may affect the protein folding and secondary structure content. Under the investigated experimental conditions, a minor loss of protein secondary structure and no aggregation of confined protein is established.

dx.doi.org/10.1021/jp303863q | J. Phys. Chem. B 2012, 116, 7676–7686

■ ASSOCIATED CONTENT

Supporting Information

Synchrotron radiation small-angle XRD data of a fully hydrated self-assembled LC sample and additional FF-EM results. This material is available free of charge via the Internet at http://pubs.acs.org.

■ AUTHOR INFORMATION

Corresponding Author

*E-mail: Angelina.Angelova@u-psud.fr.

Notes

The authors declare no competing financial interest.

■ ACKNOWLEDGMENTS

The support from the ISA User Program under the EC Grant Agreement ELISA 226716, European Community's Seventh Framework Programme (FP7/2007-2013), at the UV-VUV CD1 beamline is gratefully acknowledged. B.A. acknowledges the Czech Science Foundation Grant No. P208/10/1600. The authors thank Dr. Sergio S. Funari (HASYLAB/DESY, SAXS beamline A2, Hamburg) for continuous cooperation. The facilities at the platform "Cellular Imaging" of IFR141, Institut Paris-Sud d'Innovation Thérapeutique (IPSIT), and the programme support ANR SIMI10 Nanosciences and "Investissements d'Avenir" (French Ministry of Research and Higher Education) to the LabEx LERMIT are acknowledged.

■ REFERENCES

(1) (a) Clerc, M; Levelut, A. M.; Sadoc, J.-F. *J. Phys. II* **1991**, *1*, 1263−1276. (b) Zeng, X. B.; Ungar, G.; Imperor-Clerc, M. *Nat. Mater.* **2005**, *4*, 562−567. (c) Kulkarni, C. V.; Tang, T. Y.; Seddon, A. M.; Seddon, J. M.; Ces, O.; Templer, R. H. *Soft Matter* **2010**, *6*, 3191−3194. (d) Kulkarni, C. V. *Langmuir* **2011**, *27*, 11790−11800.

(2) (a) Hyde, S. T.; Anderson, S.; Ericsson, B.; Larsson, K. *Z. Kristallogr.* **1984**, *168*, 213−219. (b) Hyde, S. T.; de Campo, L.; Oguey, C. *Soft Matter* **2009**, *5*, 2782−2794.

(3) (a) Mariani, P.; Luzzati, V.; Delacroix, H. *J. Mol. Biol.* **1988**, *204*, 165−188. (b) Luzzati, V. *Curr. Opin. Struct. Biol.* **1997**, *7*, 661−668. (c) Razumas, V.; Larsson, K.; Miezis, Y.; Nylander, T. *J. Phys. Chem.* **1996**, *100*, 11766−11774. (d) Misiunas, A.; Talaikyté, Z.; Niaura, G.; Razumas, V.; Nylander, T. *Biophys. Chem.* **2008**, *134*, 144−156.

(4) (a) Czeslik, C.; Winter, R.; Rapp, G.; Bartels, K. *Biophys. J.* **1995**, *68*, 1423−1429. (b) Funari, S. S.; Rapp, G. *Proc. Natl. Acad. Sci. U.S.A.* **1999**, *96*, 7756−7759. (c) J. Erbes, J.; Gabke, A.; Rapp, G.; Winter, R. *Phys. Chem. Chem. Phys.* **2000**, *2*, 151−162. (d) Winter, R. *Biochim. Biophys. Acta* **2002**, *1595*, 160−184.

(5) (a) Conn, C. E.; Ces, O.; Mulet, X.; Finet, S.; Winter, R.; Seddon, J. M.; Templer, R. H. *Phys. Rev. Lett.* **2006**, *96*, 108102. (b) Sagnella, S. M.; Conn, C. E.; Krodkiewska, I.; Moghaddam, M.; Seddon, J. M.; Drummond, C. J. *Langmuir* **2010**, *26*, 3084−3094. (c) Squires, A. M.; Templer, R. H.; Seddon, J. M.; Woenckhaus, J.; Winter, R.; Finet, S.; Theyencheri, N. *Langmuir* **2002**, *18*, 7384−7392.

(6) (a) Bastos, M.; Silva, T.; Teixeira, V.; Nazmi, K.; Bolscher, J. G.; Funari, S. S.; Uhríková, D. *Biophys. J.* **2011**, *101*, L20−L22. (b) Lengyel, A.; Uhríková, D.; Klacsova, M.; Balgavy, P. *Colloids Surf., B* **2011**, *86*, 212−217. (c) Persson, G.; Edlund, H.; Amenitsch, H.; Laggner, P.; Lindblom, G. *Langmuir* **2003**, *19*, 5813−5822. (d) Clogston, J.; Caffrey, M. *J. Controlled Release* **2005**, *107*, 97−111.

(7) (a) Angelov, B.; Angelova, A.; Mutafchieva, R.; Lesieur, S.; Vainio, U.; Garamus, V. M.; Jensen, G. V.; Pedersen, J. S. *Phys. Chem. Chem. Phys.* **2011**, *13*, 3073−3081. (b) Angelov, B.; Angelova, A.; Ollivon, M.; Bourgaux, C.; Campitelli, A. *J. Am. Chem. Soc.* **2003**, *125*, 7188−7189. (c) Angelova, A.; Ollivon, M.; Campitelli, A.; Bourgaux, C. *Langmuir* **2003**, *19*, 6928−6935.

(8) (a) Kulkarni, C. V.; Wachter, W.; Iglesias-Salto, G.; Engelskirchen, S.; Ahualli, S. *Phys. Chem. Chem. Phys.* **2011**, *13*, 3004−3021. (b) Angelov, B.; Angelova, A.; Filippov, S.; Karlsson, G.; Terrill, N.; Lesieur, S.; Štěpánek, P. *J. Phys.: Conf. Ser.* **2012**, *351*, 012004. (c) Yaghmur, A.; Rappolt, M.; Østergaard, J.; Larsen, C.; Larsen, S. W. *Langmuir* **2012**, *28*, 2881−2889.

(9) (a) Angelova, A.; Angelov, B.; Mutafchieva, R.; Garamus, V. M.; Lesieur, S.; Funari, S. S.; Willumeit, R.; Couvreur, P. *Prog. Colloid Polym. Sci.* **2011**, *138*, 1−6. (b) Angelov, B.; Ollivon, M.; Angelova. *Langmuir* **1999**, *15*, 8225−8234. (c) Angelov, B.; Angelova, A.; Mutafchieva, R.; Lesieur, S.; Bourgaux, C.; Willumeit, R.; Couvreur, P. In *Nanoscience & Nanotechnology*; Balabanova, E., Dragieva, I., Eds.; Prof. Marin Drinov Academic Publishing House: Sofia, Bulgaria, 2008; Vol. *8*, pp 231−234.

(10) (a) Angelov, B.; Angelova, A.; Vainio, U.; Garamus, V. M.; Lesieur, S.; Willumeit, R.; Couvreur, P. *Langmuir* **2009**, *25*, 3734−3742. (b) Angelov, B.; Angelova, A.; Garamus, V. M.; Le Bas, G.; Lesieur, S.; Ollivon, M.; Funari, S.; Willumeit, R.; Couvreur, P. *J. Am. Chem. Soc.* **2007**, *129*, 13474−13479. (c) Angelova, A.; Angelov, B.; Garamus, V. M.; Couvreur, P.; Lesieur, S. *J. Phys. Chem. Lett.* **2012**, *3*, 445−457.

(11) (a) Kraineva, J.; Nicolini, C.; Thiyaragarajan, P.; Kondrashkina, E.; Winter, R. *Biochim. Biophys. Acta* **2006**, *1764*, 423−433. (b) Kraineva, J.; Narayanan, R. A.; Kondrashkina, E.; Thiyagarajan, P.; Winter, R. *Langmuir* **2005**, *21*, 3559−3571. (c) Yaghmur, A.; Laggner, P.; Zhang, S.; Rappolt, M. *PloS ONE* **2007**, *2*, e479.

(12) (a) Leal, C.; Ewert, K. K.; Shirazi, R. S.; Bouxsein, N. F.; Safinya, C. R. *Langmuir* **2011**, *27*, 7691−7697. (b) Leal, C.; Bouxsein, N. F.; Ewert, K. K.; C.R. Safinya, C. R. *J. Am. Chem. Soc.* **2010**, *132*, 16841−16847. (c) Zidovska, A.; Evans, H. M.; Ewert, K. K.; Quispe, J.; Carragher, B.; Potter, C. S.; Safinya, C. R. *J. Phys. Chem. B* **2009**, *113*, 3694−3703.

(13) (a) Yaghmur, A.; Kriechbaum, M.; Amenitsch, H.; Steinhart, M.; Laggner, P.; Rappolt, M. *Langmuir* **2010**, *26*, 1177−1185. (b) Gummel, J.; Sztucki, M.; Narayanan, T.; Gradzielski, M. *Soft Matter* **2011**, *7*, 5731−5738. (c) Moitzi, C.; Guillot, S.; Fritz, G.; Salentinig, S.; Glatter, O. *Adv. Mater.* **2007**, *19*, 1352−1358.

(14) (a) Marchini, C.; Montani, M.; Amici, A.; Amenitsch, H.; Marianecci, C.; Pozzi, D.; Caracciolo, G. *Langmuir* **2009**, *25*, 3013−3021. (b) McLoughlin, D.; Impéror-Clerc, M.; Langevin, D. *ChemPhysChem* **2004**, *5*, 1619−1623. (c) Shearman, G. C.; Brooks, N. J.; Tiddy, G. J. T.; Sztucki, M.; Templer, R. H.; Law, R. V.; Ces, O.; Seddon, J. M. *Soft Matter* **2011**, *7*, 4386−4390. (d) Tyler, A. I. I.; Shearman, G. C.; Brooks, N. J.; Delacroix, H.; Law, R. V.; Templer, R. H.; Ces, O.; Seddon, J. M. *Phys. Chem. Chem. Phys.* **2011**, *13*, 3033−3038.

(15) (a) Plassat, V.; Martina, M.-S.; Barratt, G.; Menager, C.; Lesieur, S. *Int. J. Pharm.* **2007**, *344*, 118−27. (b) Menager, C.; Guemghar, D.; Cabuil, V.; Lesieur, S. *Langmuir* **2010**, *26*, 15453−15463. (c) Barauskas, J.; Cervin, C.; Jankunec, M.; Špandyreva, M.; Ribokaite, K.; Tiberg, F.; Johnsson, M. *Int. J. Pharm.* **2010**, *391*, 284−291. (d) Vallooran, J. J.; Bolisetty, S.; Mezzenga, R. *Adv. Mater.* **2011**, *23*, 3932−3937.

(16) (a) Angelova, A.; Angelov, B.; Mutafchieva, R.; Lesieur, S.; Couvreur, P. *Acc. Chem. Res.* **2011**, *44*, 147−156. (b) Angelov, B.; Angelova, A.; Filippov, S.; Karlsson, G.; Terrill, N.; Lesieur, S.; Štěpánek, P. *Soft Matter* **2011**, *7*, 9714−9720.

(17) (a) Larsson, K. *Curr. Opin. Colloid Interface Sci.* **2000**, *5*, 64−69. (b) Gustafsson, J.; Ljusberg-Wahren, H.; Almgren, M.; Larsson, K. *Langmuir* **1996**, *12*, 4611−4613. (c) Gustafsson, J.; Ljusberg-Wahren, H.; Almgren, M.; Larsson, K. *Langmuir* **1997**, *13*, 6964−6971. (d) Neto, C.; Aloisi, G.; Baglioni, P.; Larsson, K. *J. Phys. Chem. B* **1999**, *103*, 3896−3899.

(18) (a) Borné, J.; Nylander, T.; Khan, A. *J. Phys. Chem. B* **2002**, *106*, 10492−10500. (b) Rosa, M.; Infante, M. R.; Miguel, M. G.; Lindman, B. *Langmuir* **2006**, *22*, 5588−5596. (c) Caboi, F.; Amico, G. S.; Pitzalis, P.; Monduzzi, M.; Nylander, T.; Larsson, K. *Chem. Phys. Lipids* **2001**, *109*, 47−62.

(19) (a) Dong, Y.-D.; Larson, I.; Hanley, T.; Boyd, B. J. *Langmuir* **2006**, *22*, 9512−9518. (b) Sagnella, S. M.; Gong, X.; Moghaddam, M. J.; Conn, C. E.; Kimpton, K.; Waddington, L. J.; Krodkiewska, I.; Drummond, C. J. *Nanoscale* **2011**, *3*, 919−924. (c) Fong, W. K.; Hanley, T.; Boyd, B. J. *J. Controlled Release* **2009**, *135*, 218−226.
(20) (a) Almgren, M.; Rangelov, S. *J. Dispersion Sci. Technol* **2006**, *27*, 599−609. (b) Almgren, M.; Borne, J.; Feitosa, E.; Khan, A.; Lindman, B. *Langmuir* **2007**, *23*, 2768−2777. (c) Almgren, M.; Edwards, K.; Gustavsson, J. *Curr. Opin. Colloid Interface Sci.* **1996**, *1*, 270−278.
(21) (a) Angelova, A.; Angelov, B.; Papahadjopoulos-Sternberg, B.; Ollivon, M.; Bourgaux, C. *Langmuir* **2005**, *21*, 4138−4143. (b) Angelova, A.; Angelov, B.; Lesieur, S.; Mutafchieva, R.; Ollivon, M.; Bourgaux, C.; Willumeit, R.; Couvreur, P. *J. Drug Delivery Sci. Technol.* **2008**, *18*, 41−45. (c) Angelova, A.; Angelov, B.; Papahadjopoulos-Sternberg, B.; Bourgaux, C.; Couvreur, P. *J. Phys. Chem. B* **2005**, *109*, 3089−3093.
(22) (a) Angelov, B.; Angelova, A.; Papahadjopoulos-Sternberg, B.; Lesieur, S.; Sadoc, J.-F.; Ollivon, M.; Couvreur, P. *J. Am. Chem. Soc.* **2006**, *128*, 5813−5817. (b) Angelova, A.; Angelov, B.; Papahadjopoulos-Sternberg, B.; Ollivon, M.; Bourgaux, C. *J. Drug Delivery Sci. Technol.* **2005**, *15*, 108−112. (c) Angelova, A.; Barbet, J.; Barratt, G.; Betbeder, D.; Moine, L. *Int. J. Pharm.* **2007**, *344*, 1−2.
(23) (a) Nakano, M.; Teshigawara, T.; Sugita, A.; Leesajakul, W.; Taniguchi, A.; Kamo, T.; Matsuoka, H.; Handa, T. *Langmuir* **2002**, *18*, 9283−9288. (b) Nakano, M.; Sugita, A.; Matsuoka, H.; Handa, T. *Langmuir* **2001**, *17*, 3917−3922. (c) Murgia, S.; Falchi, A. M.; Mano, M.; Lampis, S.; Angius, R.; Carnerup, A. M.; Schmidt, J.; Diaz, G.; Giacca, M.; Talmon, Y.; Monduzzi, M. *J. Phys. Chem. B* **2010**, *114*, 3518−3525.
(24) (a) Spicer, P. T.; Hayden, K. L.; Lynch, M. L.; Ofori-Boateng, A.; Burns, J. L. *Langmuir* **2001**, *17*, 5748−5756. (b) Spicer, P.T. In *Marcel Dekker Encyclopedia of Nanoscience and Nanotechnology*; Schwarz, J. A., Contescu, C., Putyera, K., Eds.; Marcel Dekker: New York, 2003; pp 881−892. (c) Lynch, M. L., Spicer, P. T., Eds. *Bicontinuous Liquid Crystals; Surfactant Science Series*; Taylor & Francis: Boca Raton, FL, 2005; Vol. *127*. (d) Lynch, M. L.; Ofori-Boateng, A.; Hippe, A.; Kochvar, K.; Spicer, P. T. *J. Colloid Interface Sci.* **2003**, *260*, 404−413.
(25) (a) Esposito, E.; Mariani, P.; Ravani, L.; Contado, C.; Volta, M.; Bido, S.; Drechsler, M.; Mazzoni, S.; Menegatti, E.; Morari, M.; Cortesi, R. *Eur. J. Pharm. Biopharm.* **2012**, *80*, 306−314. (b) Salentinig, S.; Yaghmur, A.; Guillot, S.; Glatter, O. *J. Colloid Interface Sci.* **2008**, *326*, 211−220. (c) Yaghmur, A.; Larsen, S. W.; Schmitt, M.; Østergaard, J.; Larsen, C.; Jensen, H.; Urtti, A.; Rappolt, M. *Soft Matter* **2011**, *7*, 8291−8295.
(26) (a) Worle, G.; Siekmann, B.; Koch, M. H. J.; Bunjes, H. *Eur. J. Pharm. Sci.* **2006**, *27*, 44−53. (b) Worle, G.; Siekmann, B.; Bunjes, H. *Eur. J. Pharm. Biopharm.* **2006**, *63*, 128−133. (c) Han, S.; Shen, J.; Gan, Y.; Geng, H.-M.; Zhang, X.; Zhu, C.-L.; Gan, L. *Acta Pharmacol. Sin.* **2010**, *31*, 990−998. (d) Gan, L.; Shun, H.; Shen, J.; Zhu, J.; Zhu, C.; Zhang, X.; Gan, Y. *Int. J. Pharm.* **2010**, *396*, 179−187. (e) Efrat, R.; Kesselman, E.; Aserin, A.; Garti, N.; Danino, D. *Langmuir* **2009**, *25*, 1316−1326.
(27) (a) Barauskas, J.; Johnsson, M.; Joabsson, F.; Tiberg, F. *Langmuir* **2005**, *21*, 2569−2577. (b) Johnsson, M.; Barauskas, J.; Tiberg, F. *J. Am. Chem. Soc.* **2005**, *127*, 1076−1077. (c) Barauskas, J.; Misiunas, A.; Gunnarsson, T.; Tiberg, F.; Johnsson, M. *Langmuir* **2006**, *22*, 6328−6334.
(28) (a) Fong, C.; Weerawardena, A.; Sagnella, S. M.; Mulet, X.; Waddington, L.; Krodkiewska, I.; Drummond, C. J. *Soft Matter* **2010**, *6*, 4727−4741. (b) Boyd, B. J.; Rizwan, S. B.; Dong, Y.-D.; Hook, S.; Rades, T. *Langmuir* **2007**, *23*, 12461−12464. (c) Lee, K. W. Y.; Nguyen, T.; Hanley, T.; Boyd, B. J. *Int. J. Pharm.* **2009**, *365*, 190−199. (d) Chong, J. Y. T.; Mulet, X.; Waddington, L. J.; Boyd, B. J.; Drummond, C. J. *Soft Matter* **2011**, *7*, 4768−4777.
(29) (a) Dong, Y.-D.; Tilley, A. J.; Larson, I.; Lawrence, M.; J. Amenitsch, H.; Rappolt, M.; Hanley, T.; Boyd, B. J. *Langmuir* **2010**, *26*, 9000−9010. (b) Vandoolaeghe, P.; Barauskas, J.; Johnsson, M.; Tiberg, F.; Nylander, T. *Langmuir* **2009**, *25*, 3999−4008.
(30) (a) Imura, T.; Yanagishita, H.; Ohira, J.; Sakai, H.; Abe, M.; Kitamoto, D. *Colloids Surf., B* **2005**, *43*, 115−121. (b) Watanabe, K.; Nakama, Y.; Yanaki, T.; Hoffmann, H. *Langmuir* **2001**, *17*, 7219−7224. (c) Imura, T.; Yanagishita, H.; Kitamoto, D. *J. Am. Chem. Soc.* **2004**, *126*, 10804−10805. (d) Meyer, H. W.; Richter, W. *Micron* **2001**, *32*, 615−644.
(31) Paleos, C. M.; Tsiourvas, D. *J. Mol. Recognit.* **2006**, *19*, 60−67.
(32) Chiruvolu, S.; Walker, S.; Leckband, D.; Israelachvili, J.; Zasadzinski, J. *Science* **1994**, *264*, 1753−1756.
(33) (a) Kisak, E. T.; Coldren, B.; Zasadzinski, J. A. *Langmuir* **2002**, *18*, 284−288. (b) Walker, S. A.; Kennedy, M. T.; Zasadzinski, J. A. *Nature* **1997**, *387*, 61−64. (c) Boyer, C. C.; Zasadzinski, J. A. *ACS Nano* **2007**, *1*, 176−182.
(34) Al-Jamal, W. T.; Kostarelos, K. *Nanomedicine* **2007**, *2*, 85−98.
(35) (a) Ye, Q.; Asherman, J.; Stevenson, M.; Brownson, E.; Katre, N. V. *J. Controlled Release* **2000**, *64*, 155−166. (b) Langston, M. V.; Ramprasad, M. P.; Kararli, T. T.; Galluppi, G. R.; Katre, N. V. *J. Controlled Release* **2003**, *89*, 87−99.
(36) (a) Nekovee, M.; Coveney, P. V. *J. Am. Chem. Soc.* **2001**, *123*, 12380−12382. (b) Saksena, R. S.; Coveney, P. V. *J. Phys. Chem. B* **2008**, *112*, 2950−2957.
(37) (a) Martina, M.-S.; Nicolas, V.; Wilhelm, C.; Menager, C.; Barratt, G.; Lesieur, S. *Biomaterials* **2007**, *28*, 4143−4153. (b) Martina, M.-S.; Wilhelm, C.; Lesieur, S. *Biomaterials* **2008**, *29*, 4137−4145.
(38) (a) Miles, A. J.; Hoffmann, S. V.; Tao, Y.; Janes, R. W.; Wallace, B. A. *Spectroscopy* **2007**, *21*, 245−255. (b) Miles, A. J.; Janes, R. W.; Brown, A.; Clarke, D. T.; Sutherland, J. C.; Tao, Y.; Wallace, B. A.; Hoffmann, S. V. *J. Synchrotron Radiat.* **2008**, *15*, 420−422. (c) Wallace, B. A.; Gekko, K.; Hoffmann, S. V.; Lin, Y.-H.; Sutherland, J. C.; Tao, Y.; Wien, F.; Janes, R. W. *Nucl. Instrum. Methods Phys. Res., Sect. A* **2011**, *649*, 177−178.
(39) (a) Wallace, B. A.; Janes, R. W. *Biochem. Soc. Trans.* **2010**, *38*, 861−873. (b) Miles, A. J.; Wallace, B. A. *Chem. Soc. Rev.* **2006**, *35*, 39−51. (c) Whitmore, L.; Wallace, B. A. *Biopolymers* **2008**, *89*, 392−400. (d) Lees, J. G.; Smith, B. R.; Wien, F.; Miles, A. J.; Wallace, B. A. *Anal. Biochem.* **2004**, *332*, 285−289.
(40) (a) Laera, S.; Ceccone, G.; Rossi, F.; Gilliland, D.; Hussain, R.; Siligardi, G.; Calzolai, L. *Nano Lett.* **2011**, *11*, 4480−4484. (b) Jorgensen, L.; Bennedsen, P.; Hoffmann, S. V.; Krogh, R. L.; Pinholt, C.; Groenning, M.; Hostrup, S.; Bukrinsky, J. T. *Eur. J. Pharm. Sci.* **2011**, *42*, 509−516.
(41) (a) Zhai, J.; Hoffmann, S. V.; Day, L.; Lee, T.-H.; Augustin, M. A.; Aguilar, M.-I.; Wooster, T. J. *Langmuir* **2012**, *28*, 2357−2367. (b) Zhai, J.; Wooster, T. J.; Hoffmann, S. V.; Lee, T.-H.; Augustin, M. A.; Aguilar, M.-I. *Langmuir* **2011**, *27*, 9227−9236. (c) Zhai, J.; Miles, A. J.; Pattenden, L. K.; Lee, T. H.; Augustin, M. A.; Wallace, B. A.; Aguilar, M. I.; Wooster, T. J. *Biomacromolecules* **2010**, *11*, 2136−2142.
(42) (a) Ambroggio, E. E.; Separovic, F.; Bowie, J. H.; Fidelio, G. D.; Bagatolli, L. A. *Biophys. J.* **2005**, *89*, 1874−1881. (b) Bernardino de la Serna, J.; Oradd, G.; Bagatolli, L. A.; Simonsen, A. C.; Marsh, D.; Lindblom, G.; Perez-Gil, J. *Biophys. J.* **2009**, *97*, 1381−1389. (c) Bagatolli, L. A. *Biochim. Biophys. Acta* **2006**, *1758*, 1541−1556.
(43) (a) Yaghmur, A.; de Campo, L.; Sagalowicz, L.; Leser, M. E.; Glatter, O. *Langmuir* **2006**, *22*, 9919−9927. (b) Yaghmur, A.; Sartori, B.; Rappolt, M. *Phys. Chem. Chem. Phys.* **2011**, *13*, 3115−3125.
(44) Fenske, D. B.; Cullis, P. R. *Methods Enzymol.* **2005**, *391*, 7−39.
(45) Ostwald, W. *Z. Phys. Chem.* **1900**, *34*, 495.
(46) de Campo, L.; Yaghmur, A.; Sagalowicz, L.; Leser, M. E.; Watzke, H.; Glatter, O. *Langmuir* **2004**, *20*, 5254−5261.
(47) Yaghmur, A.; Paasonen, L.; Yliperttula, M.; Urtti, A.; Rappolt, M. *J. Phys. Chem. Lett.* **2010**, *1*, 962−966.